Vehicle System Dynamics: International Journal of Vehicle Mechanics and Mobility

Inverse neuro-fuzzy MR damper model and its application in vibration control of vehicle suspension system

Lu-Hang Zong [a] , Xing-Long Gong [a] , Chao-Yang Guo [a] & Shou-Hu Xuan [a]

[a] CAS Key Laboratory of Mechanical Behavior and Design of Materials, Department of Modern Mechanics, University of Science and Technology of China (USTC), Hefei, 230027, People's Republic of China

PLEASE SCROLL DOWN FOR ARTICLE

Taylor & Francis
Taylor & Francis Group

Inverse neuro-fuzzy MR damper model and its application in vibration control of vehicle suspension system

Lu-Hang Zong, Xing-Long Gong*, Chao-Yang Guo, and Shou-Hu Xuan

CAS Key Laboratory of Mechanical Behavior and Design of Materials, Department of Modern Mechanics, University of Science and Technology of China (USTC), Hefei 230027, People's Republic of China

In this paper, a magneto-rheological (MR) damper-based semi-active controller for vehicle suspension is developed. This system consists of a linear quadratic Gauss (LQG) controller as the system controller and an adaptive neuro-fuzzy inference system (ANFIS) inverse model as the damper controller. First, a modified Bouc–Wen model is proposed to characterise the forward dynamic characteristics of the MR damper based on the experimental data. Then, an inverse MR damper model is built using ANFIS technique to determine the input current so as to gain the desired damping force. Finally, a quarter-car suspension model together with the MR damper is set up, and a semi-active controller composed of the LQG controller and the ANFIS inverse model is designed. Simulation results demonstrate that the desired force can be accurately tracked using the ANFIS technique and the semi-active controller can achieve competitive performance as that of active suspension.

Keywords: MR damper; ANFIS inverse model; semi-active control; LQG control; vehicle suspension

1. Introduction

In modern vehicles, vehicle suspension plays an important role in improving the ride comfort, road holding and suspension deflection. There are three types of vehicle suspensions, namely passive, semi-active and active suspensions. The commonly used passive suspension featuring an oil damper provides design simplicity and cost-effectiveness in practical application. However, due to the lack of damping force controllability, its performance is limited. The active suspension using separate actuators which can exert an independent force provides high control performance in a wide frequency range. Unfortunately, the cost and complexity of this system prohibit its commercial applications. To solve these problems, researches on vibration control using semi-active suspensions have increased significantly since semi-active suspensions can provide performance benefits over passive suspensions and without requiring large power sources and expensive hardware relative to active suspensions.

Recently, the semi-active suspension based on magneto-rheological (MR) damper has attracted more attention [1–7] because of its fast response characteristic to magnetic fields, insensitivity to temperature fluctuations or impurities in the fluid, obtainment of convenient power and wide control bandwidth. The damping force generated by the MR damper cannot be controlled directly because it depends on the input current to the MR damper and the relative velocity and displacement between the piston and the damper shell, among which only the input current can be controlled. Therefore, the designation of the damper controller is still one of the important issues in the application of a MR damper. Basically, there are three major approaches have been utilised in designing of a controller for the MR damper in literatures. The first method is based on the force feedback control by a force sensor. Dyke *et al.* [8] proposed the clipped-optimal controller firstly. The command current (voltage) varies between two states according to the comparison of the desired force and the actual force. Yoshida *et al.* [9] added a function in the clipped-optimal switching, which can control the current between zero and the maximum value. The second approach is focused on the inverse MR damper model, which is a numerical model to calculate the MR damper's required control current (voltage) based on a known control force. The third approach is based on the fuzzy controller design methodology, which has been conducted recently by many researchers [10,11]. Among them, the force feedback control-based method is the simplest, but the MR damper can only approximately generate the desired optimal control force, because the command current (voltage) is not precisely calculated and an extra force sensor is needed which will increase the complicacy and the cost. The fuzzy controller design methodology does not need the accurate models of the control object or the MR damper, but it is very challenging to establish reasonable fuzzy rules because no systematic method can be adopted. Compared with the force feedback control method and the fuzzy controller design method, the inverse MR damper model-based method has two main advantages: one is more precise command current (voltage) can be calculated to track the desired force, the other is no force sensor is needed.

During the actual application, when utilising the inverse model-based method, the MR damper works via a two-step progress. Firstly, a system controller determines the desired damping force of the MR damper according to the structure responses; then a damper controller adjusts the command current applied to the MR damper to track the desired damping force. The damper controller is usually named as the inverse model of the MR damper. Thus, the successful application of the MR damper is determined practically by two aspects: one is the accurate inverse model of the MR damper to generate the command current and the other is the selection of an appropriate control strategy.

To overcome the difficulties in building the inverse model due to the inherent hysteresis and strong nonlinearity of the MR damper, several inverse dynamic models for MR dampers to gain the command current have been proposed. Generally speaking, they can be categorised as nonparametric and parametric models. For parametric models, Wang *et al.* [12] proposed a hysteretic force-velocity model based on the symmetric and asymmetric sigmoid functions, with attractive features of decoupling the current control gain function and the hysteron function. Sakai *et al.* [13] proposed a modified LuGre model, whose inverse dynamic model can analytically determine the necessary input current. The phenomenological model [14] can accurately describe the forward behaviour of the MR dampers. However, the corresponding inverse model is difficult to obtain due to its nonlinearity and complexity. Tsang *et al.* [15] developed a simplified inverse dynamics model for the phenomenological model using the exponential function to emulate the controllable force. For non-parametric models, Choi *et al.* [16] developed a polynomial model, which can easily calculate the input current with measurable velocity and has been used in several semi-active control systems [4,17]. Liao *et al.* [18] proposed a direct identification and an inverse dynamic modeling method for MR dampers using recurrent neural networks. Wang *et al.* [19] designed a kind of nuero-fuzzy system on

the basis of adaptive neuro-fuzzy inference system (ANFIS) technology to build the inverse model. Among them the polynomial model has been technically applied in the semi-active control systems. However, the effectiveness is limited because it is not precise enough in predicting the control current. The neural network model and the ANFIS model are relatively more accurate in predicting the command current of the MR dampers. When identifying the inverse model of MR damper with ANFIS, there may exist a curse of dimensionality of fuzzy system, which will dramatically increase time consumption for training, and even the inverse model may not be identifiable. So it is crucial to design a suitable architecture for the ANFIS model. In addition, the use of the ANFIS inverse model to generate the command current in semi-active control for vehicle suspension has not been reported.

In this paper, a semi-active controller composed of a linear quadratic Gauss (LQG) controller and an ANFIS inverse model is designed for vehicle suspension with an MR damper. First, a phenomenological model (modified Bouc–Wen model) is built to characterise the forward dynamic characteristics of the MR damper based on the experimental data. Then, an inverse MR damper model is built with the ANFIS technique to determine the input current so as to gain the desired damping force. Further, a quarter-car suspension model is constructed assembling with a MR damper and a semi-active controller is designed, which consists of a LQG controller to generate the active force and an ANFIS inverse model to adjust the command current. Finally, the simulation studies are carried out and the results are analysed.

2. The modified Bouc–Wen model of the MR damper

The prototype MR damper used in this study was designed and manufactured by our group [20] (Figure 1). The damper has a ±35 mm stroke with 420 mm length in its extended position and 350 mm length in its compressed position. The maximum input current to the electromagnet is 2.5 A. The time delay of the MR damper is 10 ms.

The MTS809 TestStar Material Testing System is used to test the MR damper. In each test, the excitation is a sinusoidally varying displacement of a fixed frequency and constant amplitude. The input current to the MR damper is maintained at a constant level. The excitation frequencies are 0.5, 1, 1.5 and 2 Hz and the displacement amplitudes are 10 and 15 mm, respectively. The applied input current are from 0 to 2.5 A with increment of 0.5 A. The damping force and displacement are measured and fed to a personal computer. The velocity is obtained by differentiating the displacement.

The phenomenological model, which is proposed by Spencer *et al.* [14], can accurately predict the behaviour of the MR damper over a broad range of inputs. The simple mechanical

Figure 1.   Photograph of the MR damper.
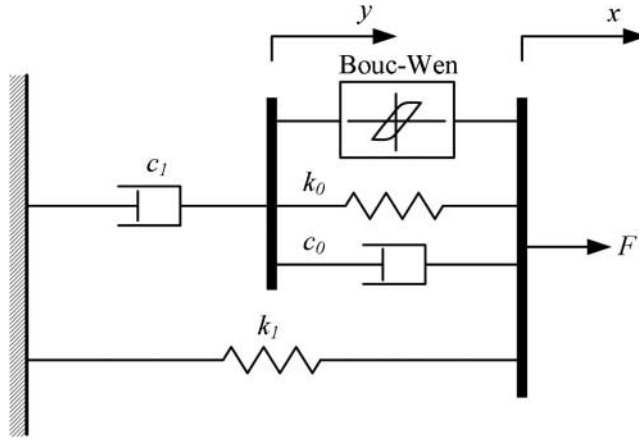
Figure 2.   The phenomenological model for the MR damper.

model of the MR damper is shown in Figure 2. It consists of mechanical elements such as springs, dashpots and hysteresis loop to emulate the device behaviour.

Here, a modified Bouc–Wen model is developed based on the phenomenological model. The model is described by the following six nonlinear differential equations:

$$F = c_1\dot{y} + k_1(x - x_0) \tag{1}$$

$$\dot{y} = \frac{1}{c_0 + c_1}[\alpha z + c_0\dot{x} + k_0(x - y)] \tag{2}$$

$$\dot{z} = -\gamma|\dot{x} - \dot{y}|z|z|^{n-1} - \beta(\dot{x} - \dot{y})|z|^n + A(\dot{x} - \dot{y}), \tag{3}$$

where F is the damping force, c_1 represents the viscous damping at low velocities, c_0 represents the viscous damping at high velocities, k_0 represents the stiffness at high velocities, k_1 is the accumulator stiffness; x is the piston relative displacement, x_0 is the initial deflection of the accumulator gas spring, y is the internal displacement of the damper and z is the evolutionary variable; α is a scaling value for the Bouc–Wen model, γ, β, A and n are parameters used to adjust the scale and shape of the hysteresis loop, respectively.

The parameters γ, β, A, n and k_1 are considered fixed and the parameters c_0, c_1 and α are assumed to be a function of the applied current I.

$$\alpha = \alpha_a + \alpha_b I, \tag{4}$$

$$c_0 = c_{0a} + c_{0b}I, \tag{5}$$

$$c_1 = c_{1a} + c_{1b}I. \tag{6}$$

The 13 parameters c_{0a}, c_{0b}, c_{1a}, c_{1b}, α_a, α_b, k_0, k_1, x_0, γ, β, A and n of every single input current are estimated at an excitation having a frequency of 2 Hz and an amplitude of 10 mm on the basis of minimising the error between the model predicted force (F_p) and the force obtained in the experiment (F_e) over one complete cycle. The error in the model is represented by the objective function E_t given by

$$E_t = \frac{\xi_t}{\sigma_F}, \tag{7}$$

Table 1. Parameter values of MR damper model.

Parameter	Values	Parameter	Values
c_{0a}	0.977 N s/mm	k_1	0.134 N/mm
c_{0b}	0 N s/mm/A	x_0	114.93 mm
c_{1a}	8.168 N s/mm	β	0.07 mm^{-2}
c_{1b}	2.725 N s/mm/A	A	300
α_a	0 N/mm	γ	0.07 mm^{-2}
α_b	1.723 N/mm/A	n	2
k_0	1.072×10^{-2} N/m	–	–

where

$$\xi_t^2 = \int_0^T (F_{\text{exp}} - F_{\text{pre}})^2 \, dt \tag{8}$$

$$\sigma_F^2 = \int_0^T (F_{\text{exp}} - \mu_F)^2 \, dt, \tag{9}$$

where μ_F is the average value of the force obtained in experiment (F_e) over one complete cycle. Optimum values of the 13 parameters have been obtained using Genetic Algorithm (GA) tool available in MATLAB® Toolboxes. The optimum values are listed in Table 1.

In order to validate the obtained modified Bouc–Wen model, the measured damping force and the predicted damping force are compared (Figure 3), where the excitation frequency and amplitude are 2 Hz and ±10 mm, respectively. The error between the measured force and the predicted force under various applied input currents, represented by the objective function E_t, are also listed in Figure 3(b). It is clearly observed that the damping force predicted by the modified Bouc–Wen model agrees well with the experiment force. It can also be seen that the accuracy in large current is better than that in small current.

3. ANFIS inverse model

The damping force generated by the MR damper is mainly decided by the input current, the piston relative velocity and the piston relative displacement. Only the input current can be directly controlled to operate the MR damper. Therefore, it is important to obtain the command current according to the desired force in actual use. In this section, ANFIS technique is applied to build the inverse MR damper model, because of its universal approximation ability to nonlinear system [21].

3.1. *ANFIS architecture*

As an example, the architecture of a two-input two-rule ANFIS is discussed (Figure 4). The ANFIS has five layers [21], in which the node functions in the same layer are of the same function family as described below: (Note that O_{ij} denotes the output of the ith node in the jth layer).

• Layer 1: Every node i in this layer is an square node with a note output defined by

$$O_{1,i} = \mu_{A_i}(x), \quad i = 1, 2 \tag{10}$$

or

$$O_{1,i} = \mu_{B_{i-2}}(y), \quad i = 3, 4,$$
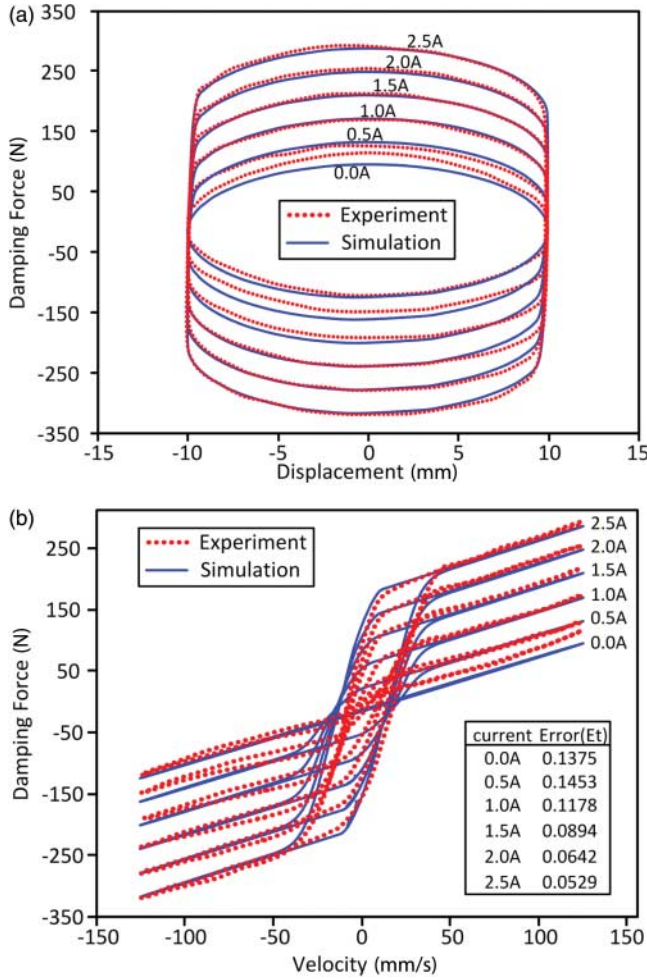
Figure 3. Comparison between the modified Bouc–Wen model and experimental results (2 Hz, ±10 mm): (a) force vs. displacement; (b) force vs. velocity.

where x (or y) is the input to node i and A_i (or B_{i-2}) is the linguistic label (*small*, *large*, etc.) associated with this node. Here, a bell-shape function with maximum equal to 1 and minimum equal to 0 is chosen, such as

$$\mu_{A_i}(x) = \frac{1}{1 + ((x - c_i)/a_i)^{2b_i}}, \tag{11}$$

where $\{a_i, b_i, c_i\}$ is the parameter set which can be changed to adjust the bell-shape function.
• Layer 2: Every node in this layer is a circle node labelled π, which multiplies the incoming signals and outputs the T-norm operator result, e.g.

$$O_{2,i} = w_i = \mu_{A_i}(x) \times \mu_{B_i}(y), \quad i = 1, 2. \tag{12}$$

Each output node represents the firing strength of a rule.
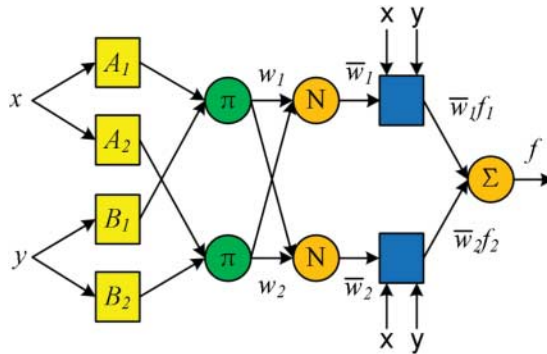
Figure 4. The architecture of a two-input two-rule ANFIS.

- Layer 3: Every node in this layer is a circle node labelled N. The ith node calculates the ratio of the ith rule's firing strength to the sum of all rules' firing strengths

$$O_{3,i} = \bar{w}_i = \frac{w_i}{w_1 + w_2}, \quad i = 1, 2. \tag{13}$$

Outputs are called normalised firing strengths.

- Layer 4: Every node i in this layer is a square node with a node function:

$$O_{4,i} = \bar{w}_i f_i = \bar{w}_i (p_i x + q_i y + r_i), \quad i = 1, 2, \tag{14}$$

where $\bar{w}_i$ is the output of layer 3 and $\{p_i, q_i, r_i\}$ is the parameter set. Parameters in this layer will be referred to as consequent parameters.

- Layer 5: The single node in this layer is labelled Σ, which computes the overall output as the summation of incoming signals, i.e.

$$O_{5,1} = \sum_{i=1}^{2} \bar{w}_i f_i = \frac{\sum_{i=1}^{2} w_i f_i}{\sum_{i=1}^{2} w_i}. \tag{15}$$

3.2. *Training inverse model*

Given input/output data sets, ANFIS constructs a fuzzy inference system (FIS) whose membership function parameters are adjusted using a hybrid algorithm. Generally speaking, the more the inputs are, the more accurate the inverse model is. However, with increase in the inputs, the inverse model will become very complex and the training time will increase enormously. To balance the model accuracy and time consumption, the inputs of the inverse model are chosen as current displacement, current velocity, previous velocity, current desired damping force and previous desired damping force, while the output is the current command current. Figure 5 shows the scheme of the ANFIS for modelling the inverse dynamics of the MR damper. The displacement input is a Gaussian white noise signal with a frequency between 0 and 13 Hz and an amplitude ± 20 mm. The command current input is generated by Gaussian white noise ranging from 0 to 3 A with a frequency of 0–6 Hz. (The purpose of choosing the maximum current as 3 A is to gain a better training result at large current around 2.5 A). The desired damping force is produced by the modified Bouc–Wen model, which is built in Section 2, according to the displacement and command current inputs. The data are collected for 20 s and sampled at 1000 Hz, therefore 20,000 points of data are generated. The first 10,000 points
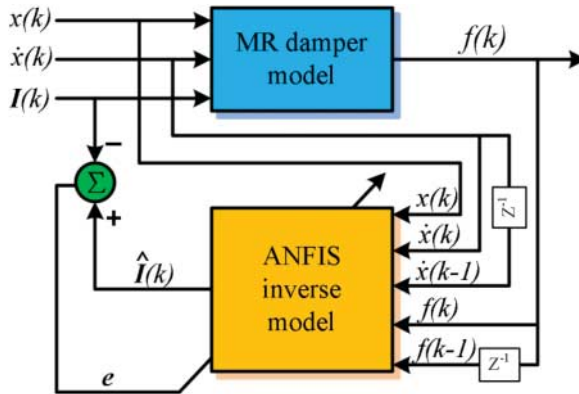
Figure 5. The scheme of the ANFIS for modeling the inverse dynamics of the MR damper.

of data are chosen to be the training data, while the later 10,000 points of data are used as checking data.

3.3. *Validation of inverse model*

In order to validate the inverse dynamic nuero-fuzzy model, three validation data sets are discussed. The first and the second validation cases are the training data and the checking data, respectively. The third validation case is the use of the ANFIS model in semi-active control for vehicle suspension system, which will be discussed in the following section. The validation flowchart of the first two cases is shown in Figure 6. Firstly, the target current, displacement and velocity are inputted to the Phenomenon model_1 to generate the target force. Then the target force, displacement and velocity are inputted to the ANFIS inverse model to generate the predicted current, and the predicted current and target current are compared in the time domain. Finally, the predicted current, displacement and velocity are inputted to the Phenomenon model_2 to generate the predicted force, and carry out the comparison between the predicted force and target force in the time domain.

The training data validation case is shown in Figure 7. It can be found that the predicted command current can track the target command current reasonably well from Figure 7(a), and the damping force produced by the predicted command current coincides with the damping force produced by the target command current from Figure 7(b).
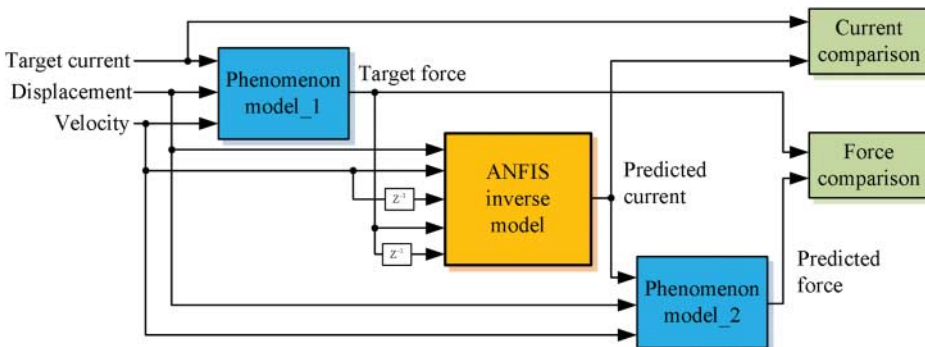
Figure 6. The validation flowchart of the ANFIS inverse model.
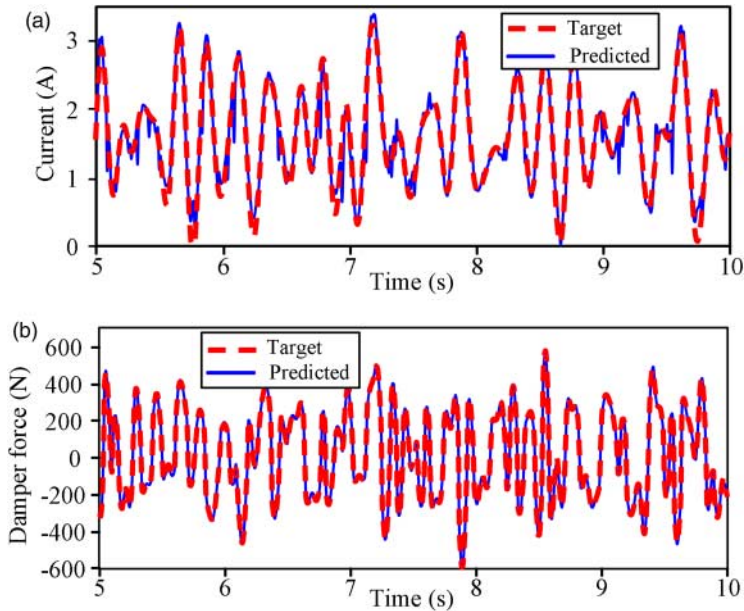
Figure 7. Validation of the ANFIS inverse model of the MR damper for training data: (a) the command current predicted by the ANFIS model and (b) the force predicted from the command current.
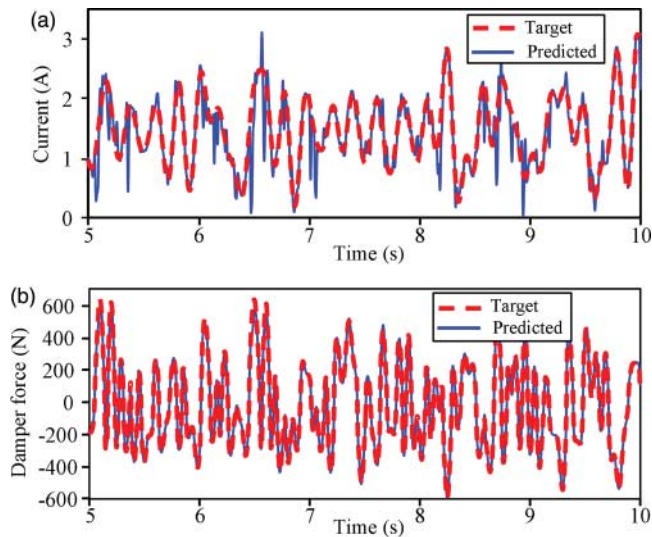
Figure 8. Validation of the ANFIS inverse model of the MR damper for checking data: (a) the command current predicted by the ANFIS model and (b) the force predicted from the command current.

The checking data validation case is shown in Figure 8. From Figure 8(a), it can be found that the accuracy of checking data is not as good as that of training data. Fortunately, it can be seen from Figure 8(b) that the damping force generated by the predicted command current can well track the damping force generated by the target command current. This can satisfy the needs for the inverse model of MR damper because the inverse model is mainly used to control the damping force of the MR damper.

4. Semi-active control of vehicle suspension system

4.1. *Vehicle suspension model*

A simple quarter-car suspension model that consists of one-fourth of the car body mass, suspension components and one wheel is studied in this work (Figure 9). The equations of motion for the sprung mass (car body mass) and unsprung mass (wheel mass) of the quarter-car suspension model are given by

$$
\begin{aligned}
m_b\ddot{x}_b + k_s(x_b - x_w) &= U(t), \\
m_w\ddot{x}_w + k_s(x_w - x_b) + k_t(x_w - x_g) &= -U(t),
\end{aligned}
\tag{16}
$$

where m_b is the sprung mass, which represents the car body; m_w is the unsprung mass, which represents the wheel assembly; k_s is the stiffness of the uncontrolled suspension system; k_t is the stiffness of the pneumatic tyre; $x_b(t)$ and $x_w(t)$ are the displacements of the sprung mass and unsprung mass, respectively; $x_g(t)$ is the road displacement input; $U(t)$ represents the external input force of the suspension system, which is generated by means of a MR damper for semi-active control.

The road irregularity input is a filtering white noise, which is governed by

$$
\dot{x}_g = -2\pi f_0 x_g + 2\pi\sqrt{G_0 U_0}\omega(t),
\tag{17}
$$

where f_0 is the low cut-off frequency, G_0 is the road irregularity coefficient, U_0 represents the car velocity and $\omega(t)$ is the Gauss white noise. Define the state variables as

$$
X = (\dot{x}_b, \dot{x}_w, x_b, x_w, x_g)^T.
\tag{18}
$$

Equations (16) and (17) can be written in state–space form as

$$
\dot{X} = AX + BU + F\omega(t),
\tag{19}
$$
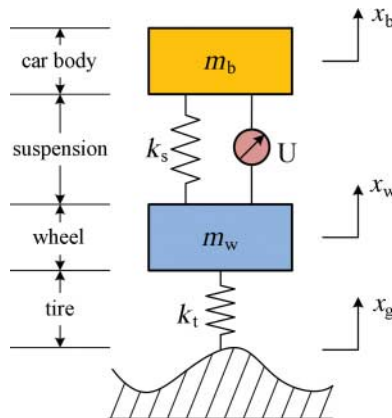
Figure 9.   Quarter-car suspension model.

where

$$
A = \begin{bmatrix}
0 & 0 & \dfrac{-k_s}{m_b} & \dfrac{k_s}{m_b} & 0 \\
0 & 0 & \dfrac{k_s}{m_w} & \dfrac{-(k_s + k_t)}{m_w} & \dfrac{k_t}{m_w} \\
1 & 0 & 0 & 0 & 0 \\
0 & 1 & 0 & 0 & 0 \\
0 & 0 & 0 & 0 & -2\pi f_0
\end{bmatrix}, \quad
B = \begin{bmatrix}
\dfrac{1}{m_b} \\
-\dfrac{1}{m_w} \\
0 \\
0 \\
0
\end{bmatrix}, \quad
F = \begin{bmatrix}
0 \\
0 \\
0 \\
0 \\
2\pi \sqrt{G_0 U_0}
\end{bmatrix}.
$$

4.2. *Formulation of LQG controller*

The optimal linear quadratic regulator (LQR) in combination with Kalman filter-based state estimation, leading to LQG optimal control, is used to calculate the optimal control force in real time. Ride comfort, road-holding ability and suspension deflection are the three main performance criteria in vehicle suspension design. Ride comfort is closely related to the vertical acceleration of the car body. In order to improve the three performance criteria and limit the magnitude of the control force, an LQR control problem is formulated. The performance function J is defined as follows:

$$
J = \lim_{x \to \infty} \frac{1}{T} \int_0^T [q_1(x_w - x_g)^2 + q_2(x_b - x_w)^2 + \ddot{x}_b^2 + rU] \, dt, \tag{20}
$$

where q_1, q_2 and r represent the weighting coefficients of road holding ability, suspension deflection and control force, respectively. The coefficient of the ride comfort is set to 1.

Rewrite the target performance evaluation function as

$$
J = \lim_{x \to \infty} \frac{1}{T} \int_0^T (X^T Q X + U^T R U + 2X^T N U) \, dt, \tag{21}
$$

where

$$
Q = \begin{bmatrix}
0 & 0 & 0 & 0 & 0 \\
0 & 0 & 0 & 0 & 0 \\
0 & 0 & \dfrac{k_s^2}{m_b^2} + q_2 & -\dfrac{k_s^2}{m_b^2} - q_2 & 0 \\
0 & 0 & -\dfrac{k_s^2}{m_b^2} - q_2 & \dfrac{k_s^2}{m_b^2} + q_1 + q_2 & -q_1 \\
0 & 0 & 0 & -q_1 & q_1
\end{bmatrix}, \quad
N = \begin{bmatrix}
0 \\
0 \\
-\dfrac{k_s}{m_b^2} \\
\dfrac{k_s}{m_b^2} \\
0
\end{bmatrix}, \quad
R = \frac{1}{m_b^2} + r,
$$

where Q is the weighting matrix of state variables, R the weighting matrix of control variables and N the weighting matrix of the cross term of state variables and control variables.

The solution to the optimal control problem that minimises this given performance index is a state feedback law $U = -GX$, where the feedback gain G is determined by solving the following Riccati equation:

$$
AP + PA^T - PBR^{-1}B^T P + Q = 0, \tag{22}
$$

$$
G = R^{-1}(N^T + B^T P). \tag{23}
$$

Considering practical application, only the suspension deflection $x_b(t) - x_w(t)$ and the acceleration of sprung mass $\ddot{x}_b(t)$ can be easily measured. But all of the state variables are needed in the LQR controller. So it is necessary to estimate all of the state variables from the measurable signals using Kalman filter-based state estimation. For this purpose, the performance function of the Kalman filter is defined as follows:

$$J_e = \lim_{x \to \infty} \frac{1}{T} \int_0^T [\{X(t) - \hat{X}(t)\}^T \{X(t) - \hat{X}(t)\}] \, dt, \tag{24}$$

where $\hat{X}(t)$ is the estimation of the state $X(t)$. The Kalman filter is represented as follows:

$$\begin{aligned}
\dot{\hat{X}} &= A\hat{X} + BU + K_e(Y - \hat{Y}), \quad \hat{X}(t_0) = \hat{X}_0, \\
\hat{Y} &= C_0\hat{X},
\end{aligned} \tag{25}$$

where K_e is the gain of Kalman filter, which is determined by solving the following Riccati equation:

$$AP_e + P_e A^T - P_e C_0^T R_e^{-1} C_0 P_e + Q_e = 0, \tag{26}$$

$$K_e = P_e C_0^T R_e^{-1}, \tag{27}$$

where $Q_e = q_e$, $R_e = r_e \times \text{eye}(2, 2)$, eye(2,2) is a 2×2 unit matrix.

Finally, the optimal control force of the system can be expressed as the feedback of the state estimation

$$U(t) = -G\hat{X}(t). \tag{28}$$

4.3. *Semi-active control system*

Because the MR damper is a semi-active device, there are two intrinsic constraints due to the characteristics of the MR dampers: the passivity constraint and the limitation constraint. In active control, forces can be produced in any of the four quadrants in the force–velocity graph, while semi-active devices can only produce forces in the first and third quadrants because of the passivity constraint. In other words, only when the active control force has the same sign to that of the MR damper's piston relative velocity, it can be produced by the MR damper. In addition to the passivity constraint, there is an upper limit and a lower limit on the force that the MR damper can produce at every moment (Figure 10), due to the actual constraint of the input current to the MR damper. In summary, only if the active control force satisfies the above two constraints, the MR damper can generate corresponding force by adjusting the input current. Otherwise, the desired damping force is either of the lower or upper level by setting the input current at either zero or the maximum achievable level, respectively. So a force limiter is designed to calculate the desired damping force according to the active control force and the suspension velocity, which is governed by

$$F_{\text{desired}} = \begin{cases} F_{\text{max}}, & F_{\text{active}} \geq F_{\text{max}}, \\ F_{\text{active}}, & F_{\text{max}} > F_{\text{active}} > F_{\text{min}}, \\ F_{\text{min}}, & F_{\text{active}} \leq F_{\text{min}}, \end{cases} \tag{29}$$
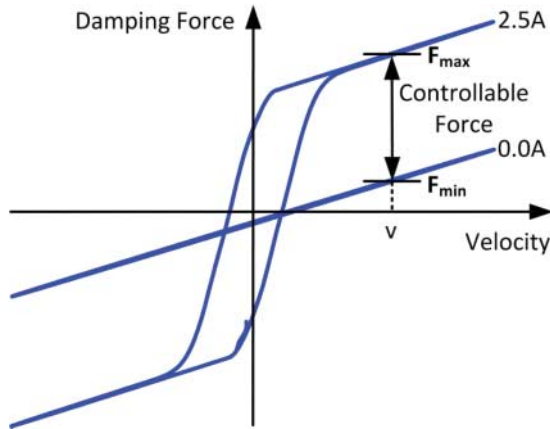
Figure 10. The scheme of controllable force.

where F_{max} is the maximum force that the MR damper can generate at present moment, F_{min} the minimum force that the MR damper can generate at present moment, F_{active} the active control force calculated by the active control algorithm and $F_{desired}$ the desired damping force that the MR damper can track.

The semi-active control system consists of a system controller and a damper controller. The system controller generates the desired damping force according to the dynamic responses of the suspension while the damper controller adjusts the input current to track the desired damping force. In this paper, the semi-active controller is composed of a LQG controller (system controller) and an ANFIS inverse model (damper controller). The structure of the semi-active controller for vehicle suspension with an MR damper is depicted in Figure 11. Firstly, the active control force is calculated by the LQG controller according to the measured outputs. Then, the desired damping force is generated by the force limiter based on the active control force. Thirdly, the ANFIS inverse model of the MR damper is used to adjust the command current according to the desired damping force and the vehicle suspension responses. Finally, the desired damping force is approximately realised by the MR damper with an appropriate input current calculated from the ANFIS inverse model.
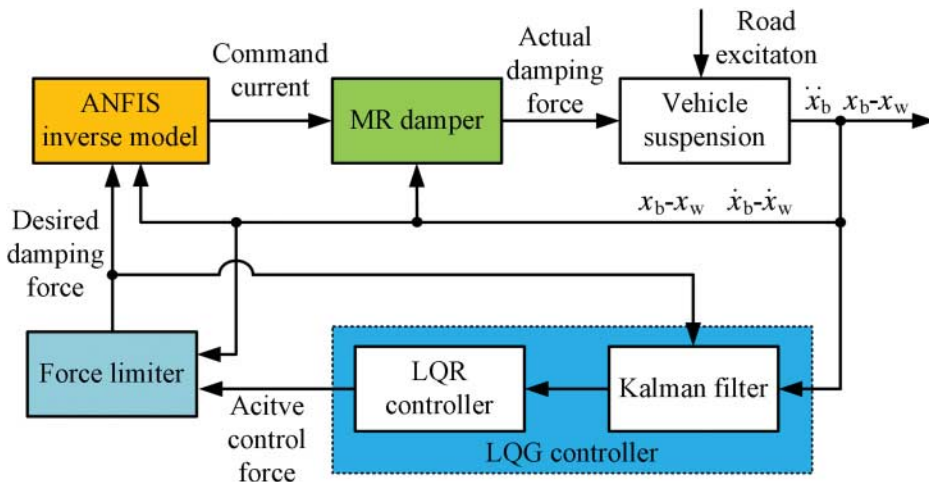
Figure 11. The structure of the semi-active controller for vehicle suspension with the MR damper.

4.4. *Simulation results*

In order to evaluate the performance of the semi-active controller with MR damper, three types of suspensions, namely passive, active and semi-active suspension, are studied in this work. Passive suspension means that the control input current to the MR damper $I(t) = 0$ A for all time, namely the passive damping is equal to 977 Ns/m. Active suspension means that the control input $U(t)$ is fully realised by Equation (28). Semi-active suspension means that the control input $U(t)$ is realised by the MR damper with the control structure in Figure 11.

The simulation parameter values are listed in Table 2. The total simulation time is 20 s, and the time step is 1 ms. The response time of the MR damper is 10 ms. The input current of the MR damper is restricted within $0 \sim 2.5$ A.

The random road excitation, the responses of the suspension system under random excitation of passive, semi-active and active suspension, the damping force and the input current to MR damper are shown in Figure 12. The displacement of the road excitation is shown in Figure 12(a). The responses of the car body acceleration, the suspension deflection and the tyre deflection are shown in Figure 12(b)–(d), respectively. Figure 12(e) shows the comparison of the actual damping force, the desired damping force and the active force. Figure 12(f) shows the input current to the MR damper of the semi-active suspension.

From Figure 12(b)–(d), it can be seen that both active and semi-active suspension systems can achieve relatively lower magnitude for car body acceleration, suspension deflection and tyre deflection when compared with the passive suspension system. Using the presented control structure (Figure 11), the semi-active suspension system together with the MR damper can achieve a control performance that is similar to that of the active suspension system except for a little deterioration because of the passivity and the limitation constraints (Figure 12(e) and 12(f)). It demonstrates the effectiveness of the semi-active controller with MR damper for vibration suppression of the suspension system.

From Figure 12(e), it can be found that the actual damping force generated by the MR damper can track the desired damping force well, which further demonstrates that the ANFIS inverse model of the MR damper is effective in controlling the damping force.

The root-mean-square (RMS) values and the peak-to-peak values of the responses are presented in Table 3. It can be seen that the active and semi-active suspension systems have good performance in car body acceleration, suspension deflection and tyre deflection than that of passive suspension system. The semi-active suspension system with the MR damper has a little deterioration of control performance in car body acceleration and tyre deflection when

Table 2. The simulation parameters values.

	Parameters	Units	Values
Vehicle suspension	m_b	kg	360
	m_w	kg	40
	k_s	Ns/m	2.0×10^4
	k_t	Ns/m	2.0×10^5
Road excitation	f_0	Hz	0.01
	G_0	m^3/cycle	5.0×10^{-6}
	U_0	m/s	20
LQR controller	q_1	–	5.0×10^4
	q_2	–	1.0×10^3
	r	–	1.0×10^{-6}
Kalman filter	q_e	–	10
	r_e	–	1.0×10^{-6}
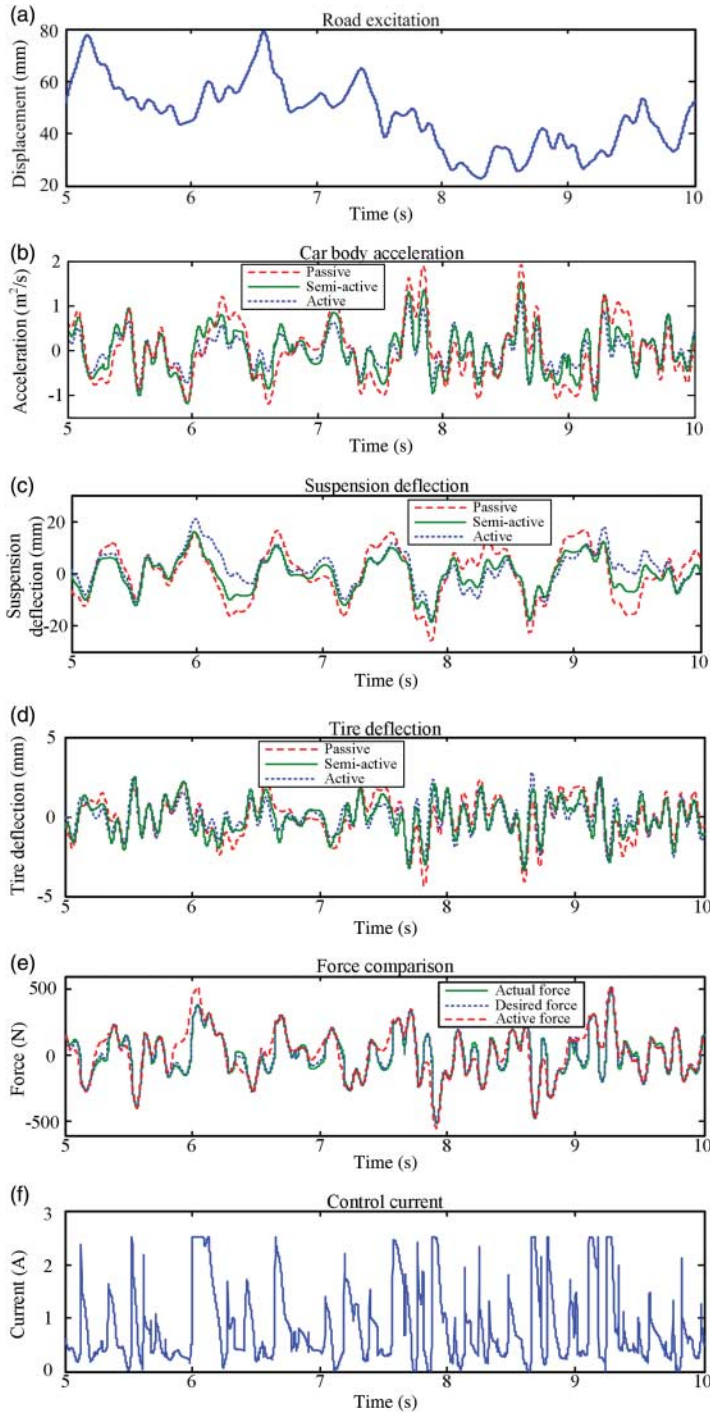
Figure 12. Suspension responses under random road excitation. (a) the displacement of the road excitation; (b) the responses of the car body acceleration; (c) the responses of the suspension deflection; (d) the responses of the tyre deflection; (e) comparison of the actual damping force, the desired damping force and the active force; (f) the input current to MR damper of the semi-active suspension.

Table 3.   RMS values and peak-to-peak values analysis.

	RMS values			Peak-to-peak values		
	Passive	Active	Semi-active	Passive	Active	Semi-active
Car body acceleration (m/s^2)	0.615	0.361	0.523	4.076	2.425	3.276
Suspension deflection (mm)	9.123	6.967	6.776	55.410	41.193	41.271
Tyre deflection (mm)	1.245	1.003	1.116	8.750	6.465	7.456

compared with that of active suspension system. But the control performance in suspension deflection of semi-active suspension is similar to that of active suspension. All these results indicate that the semi-active controller presented in this paper can work well under random excitation.

5.   Conclusions

In this paper, a semi-active controller based on the ANFIS technique for the MR damper is proposed and applied to a quarter-car vehicle suspension. The LQG controller and the ANFIS inverse model are used to generate the active force and adjust the command current, respectively. First, a modified Bouc–Wen model is used to build the forward MR damper model according to the experimental data. Then, ANFIS technique is applied to build the inverse MR damper model. The architecture and the training method for the inverse model of the MR damper are presented. Validation results show that the inverse model is effective in controlling the damping force of the MR damper. Together with the ANFIS inverse model of the MR damper and a suitably designed LQG controller, a semi-active controller is proposed and applied to a quarter-car suspension model. The performances of this controller are validated by numerical simulations. Results show that the semi-active controller can achieve compatible performance as that of active suspension controller except for a little deterioration. These results presented in this paper are still preliminary for modelling and control of the MR damper using ANFIS technique, more experimental research work is needed in order to further test the controller.

Acknowledgements

References

[1] M. Ahmadian and J.C. Poynor, *An evaluation of magneto rheological dampers for controlling gun recoil dynamics*, Shock Vib. 8(3–4) (2001), pp. 147–155.
[2] S.B. Choi, H.S. Lee, and Y.P. Park, *H(infinity) control performance of a full-vehicle suspension featuring magnetorheological dampers*, Veh. Syst. Dyn. 38(5) (2002), pp. 341–360.
[3] Z.D. Xu, Y.P. Shen, and Y.Q. Guo, *Semi-active control of structures incorporated with magnetorheological dampers using neural networks*, Smart Mater. Struct. 12(1) (2003), pp. 80–87.
[4] H.P. Du, K.Y. Sze, and J. Lam, *Semi-active H-infinity control of vehicle suspension with magneto-rheological dampers*, J. Sound Vibr. 283(3–5) (2005), pp. 981–996.
[5] X.B. Song, M. Ahmadian, S. Southward, and L.R. Miller, *An adaptive semiactive control algorithm for magnetorheological suspension systems*, J. Vib. Acoust.-Trans. ASME 127(5) (2005), pp. 493–502.
[6] M. Biglarbegian, W. Melek, and F. Golnaraghi, *A novel neuro-fuzzy controller to enhance the performance of vehicle semi-active suspension systems*, Veh. Syst. Dyn. 46(8) (2008), pp. 691–711.

 [7] C.M.D. Wilson and M.M. Abdullah, *Structural vibration reduction using self-tuning fuzzy control of magnetorheological dampers*, Bull. Earthquake Eng. 8(4) (2010), pp. 1037–1054.
 [8] S.J. Dyke, *Acceleration Feedback Control Strategies for Active and Semi-active Control Systems: Modeling, Algorithm Development, and Experimental Verification*, University of Notre Dame, Notre Dame, 1996.
 [9] O. Yoshida and S.J. Dyke, *Seismic control of a nonlinear benchmark building using smart dampers*, J. Eng. Mech.-ASCE 130(4) (2004), pp. 386–392.
[10] K.C. Schurter and P.N. Roschke, *Neuro-fuzzy control of structures using acceleration feedback*, Smart Mater. Struct. 10(4) (2001), pp. 770–779.
[11] K.M. Choi, S.W. Cho, H.J. Jung, and I.W. Lee, *Semi-active fuzzy control for seismic response reduction using magnetorheological dampers*, Earthquake Eng. Struct. Dyn. 33(6) (2004), pp. 723–736.
[12] E.R. Wang, X.Q. Ma, S. Rakhela, and C.Y. Su, *Modelling the hysteretic characteristics of a magnetorheological fluid damper*, Proc. Inst. Mech. Eng. Part D-J. Automob. Eng. 217(D7) (2003), pp. 537–550.
[13] C. Sakai, H. Ohmori, and A. Sano, *Modeling of MR Damper with Hysteresis for Adaptive Vibration Control*, 42nd IEEE Conference on Decision and Control, Maui, 2003.
[14] B.F. Spencer, S.J. Dyke, M.K. Sain, and J.D. Carlson, *Phenomenological model for magnetorheological dampers*, J. Eng. Mech.-ASCE 123(3) (1997), pp. 230–238.
[15] H.H. Tsang, R.K.L. Su, and A.M. Chandler, *Simplified inverse dynamics models for MR fluid dampers*, Eng. Struct. 28(3) (2006), pp. 327–341.
[16] S.B. Choi, S.K. Lee, and Y.P. Park, *A hysteresis model for the field-dependent damping force of a magnetorheological damper*, J. Sound Vibr. 245(2) (2001), pp. 375–383.
[17] X.M. Dong, M. Yu, Z.S. Li, C.R. Liao, and W.M. Chen, *Neural network compensation of semi-active control for magneto-rheological suspension with time delay uncertainty*, Smart Mater. Struct. 18(1) (2009), pp. 015014.
[18] D.H. Wang and W.H. Liao, *Modeling and control of magnetorheological fluid dampers using neural networks*, Smart Mater. Struct. 14(1) (2005), pp. 111–126.
[19] H. Wang and H.Y. Hu, *The fuzzy approximation of MR damper (in Chinese)*, J. Vib. Eng. 19(1) (2006), pp. 31–36.
[20] C.Y. Guo, L.H. Zong, X.M. Chen, J.F. Li, Q. Xue, and X.L. Gong, *Vibration control with an inner-pass magnetorheological damper (in Chinese)*, J. Vib. Shock, 30(3) (2011), pp. 47–52.
[21] J.S.R. Jang, *ANFIS - Adaptive-network-based fuzzy inference system*, IEEE Trans. Syst. Man Cybern. 23(3) (1993), pp. 665–685.